Chemical Geology 665 (2024) 122304

Contents lists available at ScienceDirect

Chemical Geology

journal homepage: www.elsevier.com/locate/chemgeo

Thermodynamic and kinetic considerations of the link between underground hydrogen storage and reductive carbonate dissolution and methane production. Are limestone reservoirs unsuitable for UHS?

Stephanie Vialle, Domenik Wolff-Boenisch *

School of Earth and Planetary Sciences, Curtin University, GPO Box U1987, Perth, WA-6845, Australia

ARTICLE INFO

Editor: Dr. Oleg Pokrovsky

Keywords:
Underground hydrogen storage
Reductive carbonate dissolution
Hydrogenotrophic methanation
Redox potential
Gibbs free energy

ABSTRACT

Storing hydrogen underground for cyclic injection/retrieval may help move the world towards a decarbonised economy. In search of suitable long-term reservoirs, the potential reactivity of the matrix with hydrogen plays a major role. This is especially poignant for carbonate minerals, due to their abundance, ubiquity, and much faster dissolution kinetics compared to silicates. Geochemical modelling studies invariably find hydrogen-induced reductive carbonate dissolution and methane production (HIRCDAMP) whereas experimental studies, for the most part, do not support this view. To answer the question of how far injected hydrogen may oxidise, protonate and cause reductive dissolution of carbonates, a thermodynamic approach based on standard redox and overall cell potentials, as well as Gibbs free energies, was chosen. Together with observations on kinetic constraints, a consistent picture emerges in which purely inorganically driven reduction of (bi)carbonate to methane by hydrogen oxidation is not likely to occur. Rather, the formation of intermediate carbon species (e.g., formate) could be a kinetically and thermodynamically more favourable pathway than that to methane. It follows that geochemical models that question the long-term viability of hydrogen injection into carbonate-bearing reservoirs need to be revised, toning down any alleged, yet by experimental studies not substantiated, hydrogen reactivity in the absence of any catalyst and/or microbial activity.

1. Introduction

Underground hydrogen storage (UHS), when based on hydrogen produced by the surplus of renewable energies, is being considered a promising tool to usher in an era of low carbon economy (Hanley et al., 2018). The studies reviewing the major technical hurdles of and opportunities for UHS have proliferated to a bewildering degree in recent years (Epelle et al., 2022; Hanley et al., 2018; Heinemann et al., 2021; Hematpur et al., 2023; Miocic et al., 2023; Muhammed et al., 2022; Pan et al., 2021; Raza et al., 2022; Sambo et al., 2022; Tarkowski, 2019; Tarkowski and Uliasz-Misiak, 2022; Thiyagarajan et al., 2022; Zivar et al., 2021). Among them features the quest of finding a suitable reservoir combining a connected large storage volume, enabling repeated quantitative hydrogen injection/retrieval cycles, with a tight overlying seal to keep the buoyant and diffusive hydrogen gas safely underground. Like in the case of carbon storage, much effort has been focused on deep saline aquifers and depleted oil and gas reservoirs (Krevor et al., 2023; Muhammed et al., 2022; Pan et al., 2021; Reitenbach et al., 2015; Zeng et al., 2023; Zivar et al., 2021). Most of the associated rock matrices will contain carbonates, either as primary phases (e.g., limestone or dolomite formations) or secondary phases (e.g., carbonates formed during diagenetic or post-diagenetic alterations of magmatic minerals and rock cementation). Whatever their origin and abundance, carbonate minerals are chemically far less stable than silicates and their associated siliciclastic matrices and thus more prone to chemical mobilisation, potentially induced by injection of hydrogen underground. Carbonates are hence of particular interest and concern when anticipating the long-term stability of any carbonate-bearing or cemented hydrogen storage reservoir. Alas, the literature on the reactivity of carbonates in the presence of hydrogen is inconsistent. A couple of experimental studies conclude that the presence of dissolved hydrogen promotes carbonate dissolution. Flesch et al. (2018) observed carbonate (and anhydrite) cement alteration of Triassic/Permian sandstones in the presence of hydrogen. Similarly, Bensing et al. (2022) reported hydrogen-induced calcite dissolution in claystones. These experimental findings are backed by numerical simulations that

* Corresponding author.
E-mail addresses: stephanie.vialle@curtin.edu.au (S. Vialle), Domenik.Wolff-Boenisch@curtin.edu.au (D. Wolff-Boenisch).

https://doi.org/10.1016/j.chemgeo.2024.122304
Received 19 May 2024; Received in revised form 26 July 2024; Accepted 31 July 2024
Available online 3 August 2024

invariably end up dissolving carbonates in the presence of hydrogen. For example, Hassannayebi et al. (2019) carried out geochemical modelling on a case site and found carbonates (dolomite and ankerite) dissolving within months, and concomitant hydrogen loss. Likewise, Bo et al. (2021), using geochemical modelling, reported calcite dissolution induced by hydrogen dissociation and fluid protonation, resulting in the loss of up to 9.5% hydrogen from a sedimentary reservoir rich in calcite cement. Similarly, Zeng et al. (2022) concluded after numerical modelling that carbonate reservoirs may not be suitable for long-term storage due to sustained loss of hydrogen via carbonate dissolution and methane production. On the same modelling premises and outcomes, Zhan et al. (2024) suggested focusing UHS on sandstone reservoirs where the absence of reactive carbonate phases would cause less hydrogen loss. Finally, another modelling study established that sandstone is a suitable UHS as long as the amount of calcite in the sandstone is not significant (Gholami, 2023). In contrast, other experimental studies do not substantiate this modelling pathway. Al-Yaseri et al. (2023) did not detect any methane via gas chromatography (GC) after four months of intimate hydrogen-limestone interaction at 100 bar pH_2 and 75 °C, an observation in accordance with Hassanpouryouzband et al. (2022), a source that carried out over 250 batch experiments with $H_{2(aq)}$ on six different sandstone matrices, all containing varying wt% abundances of calcite and/or dolomite. That study went over two to six weeks and did not report a single occurrence of methane in their GC analyses either. Furthermore, reacting hydrogen, albeit in its gaseous rather than dissolved state, with either $CO_{2(g)}$ (Sabatier reaction) or diverse carbonate minerals to generate methane has proven to occur only under high *P-T* conditions (hundreds of MPa and °C) and/or in the presence of specific catalytic surfaces (Giardini and Salotti, 1969; Jagadeesan et al., 2009; Mao et al., 2022; Peng et al., 2021; Rönsch et al., 2016; Scott et al., 2004; Yoshida et al., 1999). These *P-T* conditions are considerably above what can be expected under UHS reservoir conditions -and numerical simulations. A recent advance in this discussion comes from Gelencsér et al. (2023) who carried out a combined experimental-modelling study investigating the reactivity of hydrogen on calcite. Their batch experiments under elevated hydrogen storage conditions (105 °C, 100 bar) found no chemical or morphological indication of increased calcite dissolution in hydrogen atmosphere compared to blank results with nitrogen. The authors went on to carry out PHREEQC modelling of their experiments, resulting in extensive calcite dissolution and methane formation and concluded that thermodynamic databases of geochemical modelling must be reviewed for UHS. However, the study remains empirical in its approach and does not provide any explanation for the inconsistency other than observing that reductive carbonate dissolution in the presence of hydrogen only proceeds in the presence of a catalyst (e.g., Pd), not expected to be present in the UHS reservoir, or at *T-P* conditions not realised in UHS settings. Given the apparent discrepancy in deducing the potential (or lack thereof) of reductive dissolution and methanation in the presence of hydrogen, this paper sets out to explore this matter further, from a thermodynamic point of view. Its aim is to provide a theoretical footing for the likelihood of hydrogen-induced reductive carbonate dissolution and methane production (the acronym HIRCDAMP will be used in the remainder of the text). This theoretical foundation is key in characterising the link between underground hydrogen storage/retrieval and hydrogen loss via reductive carbonate dissolution so important for a successful transition towards a decarbonised economy.

2. Theoretical background

Given that T and P can be assumed constant in a given potential storage reservoir for hydrogen, the most useful thermodynamic potential that will inform on the spontaneity of a geochemical reaction is the Gibbs energy G. At standard conditions (25 °C, gases acting ideally and at a pressure of 1 bar and solutes acting ideally and at a concentration of 1 mol, which translates in the system considered in this paper as pO_2 and $pH_2 = 1$ and pH = 0), the change in Gibbs energy $\Delta_r G^o$ of a chemical reaction can be computed from the standard free Gibbs energies of formation of the different elements:

$$\Delta_r G^o = \sum_i \zeta_i . \Delta_f G_i^0, \tag{1}$$

where i refers to the element i, ζ_i to its stoichiometric coefficient and $\Delta_f G_i^0$ to its standard free Gibbs energies of formation, tabulated in databases such as the NIST Standard Reference Database (NIST, 2013). Most often, Gibbs energies are recast in the guise of the equilibrium constants K for a particular chemical reaction. K is related to the standard Gibbs energy of reaction by:

$$\Delta_r G^o = -RTln(K) = -2.303\, RT\, log(K) \tag{2}$$

with R being the gas constant and T the temperature in Kelvin.

For redox species, it is common to work with the potential difference measured in an electrolytic cell. The standard potential E^0 of the cell is obtained from the standard Gibbs energy of reaction by:

$$\Delta_r G^o = -nF\, E^0 = -nF\, \left(E^0_{\mathrm{Red}} - E^0_{\mathrm{Ox}}\right) \tag{3}$$

with n being the number of electrons exchanged between the reducing and oxidising species, F the Faraday constant, E^0_{Red} the standard half-cell potential associated with the reduction and E^0_{Ox} the standard half-cell potential associated with the oxidation.

Standard quantities are tabulated reference points used to infer the thermodynamic driving force of the chemical reactions. However, hydrogen storage reservoirs containing carbonates will exhibit conditions far from the standard ones, with pH rather alkaline and pH_2 far greater than 1 bar. For a given chemical system, with gases at partial pressures p_{gi}, solutes at molalities m_i and temperature T (different from 298 K), the Gibbs energy of reaction is then:

$$\Delta_r G_T = \Delta_r G_T^0 + 2.303\, RTlog(Q) = -2.303\, RT\, log(K_T/Q) \tag{4}$$

with

$$Q = \prod_i p_{gi}^{\zeta i} . m_i^{\nu i} \tag{5}$$

and

$$\Delta_r G_T^0 = -2.303\, RTlog(K_T) = \sum_i \zeta_i . \Delta_f G^0_{T,i} \tag{6}$$

$$\Delta_f G^0_{T,i} = \Delta_f G^0_{298,i} - \Delta_f S^0_{298,i}\, (T - 298) \tag{7}$$

with ζi and νi the stoichiometric coefficients of gas i and solute i, respectively. Eq. (6) assumes that $\Delta_f S^0_{298,i}$, the entropy of the formation of each compound i, is constant over the temperature range considered. $\Delta_f S^0_{298,i}$ can be computed from their enthalpies of formation and free Gibbs energy of formation:

$$\Delta_f S^0_{i,298} = \frac{\Delta_f G^0_{298} - \Delta_f H^0_{298}}{298} \tag{8}$$

Similarly, the redox potential at temperature T can be calculated by the expression below, known as the Nernst Equation:

$$E_T = E_T^0 - 2.303 \frac{RT}{nF} log(Q) \tag{9}$$

with

$$\Delta_r G_T^0 = -nFE_T^0 \tag{10}$$

Expressions (4) and (9) show that the Gibbs energies of reactions (or equivalently the redox potentials) will be a function of the partial pressure of H_2 and pH (and of any other gases or solutes present in the reservoir).

In the following paragraphs, we will use this thermodynamical

framework to investigate the likelihood of reductive carbonate dissolution and methanation reactions in typical conditions found in UHS. But first, we will discuss what we can learn from Pourbaix diagrams and standard thermodynamic quantities and then compare HIRDCAMP at low versus high partial pressure of H_2.

3. Theoretical deliberations

It is instructive to start the thermodynamic discussion with a review of the Pourbaix diagram of water (Fig. 1). The stability field of water is bounded by two lines that represent the redox reactions of water. Under acidic conditions, the oxidation and reduction of water are written as:

$$O_{2(g)} + 4H^+ + 4\,e^- = 2H_2O \quad (11)$$

and

$$2H^+ + 2e^- = H_{2(g)} \quad (12)$$

while under alkaline conditions, these reactions become:

$$O_{2(g)} + 2H_2O + 4\,e^- = 4OH^- \quad (13)$$

and

$$2H_2O + 4\,e^- = H_{2(g)} + 2OH^- \quad (14)$$

The upper stability limit of water (i.e., under highly oxidising conditions) is set by the oxidation of oxygen bound in water under acidic conditions (Eq. (11)) and the oxidation of oxygen bound in hydroxide under alkaline conditions (Eq. (13)). In both cases, oxidation results in the formation of elemental gaseous oxygen ($O_{2(g)}$). Its lower stability limit (i.e., under highly reducing conditions) is defined by the reduction of protons (more properly, hydrogen bound in hydronium) under acidic conditions (Eq. (12)) and the reduction of hydrogen bound in water under alkaline conditions (Eq. (14)). In both cases, reduction results in the formation of elemental gaseous hydrogen ($H_{2(g)}$). At standard conditions (25 °C, pO_2 and $pH_2 = 1$ bar, pH = 0), the redox potential corresponds to the standard reduction potential when the slope of the Nernst equation (−0.059·pH) crosses the vertical axis at pH = 0, yielding $Eh = E^0$. This is pertinent to this discussion because to understand the driving force of Eq. (12), which describes the reactive nature of dissolved hydrogen and its potential to act as an acid and reducing agent,

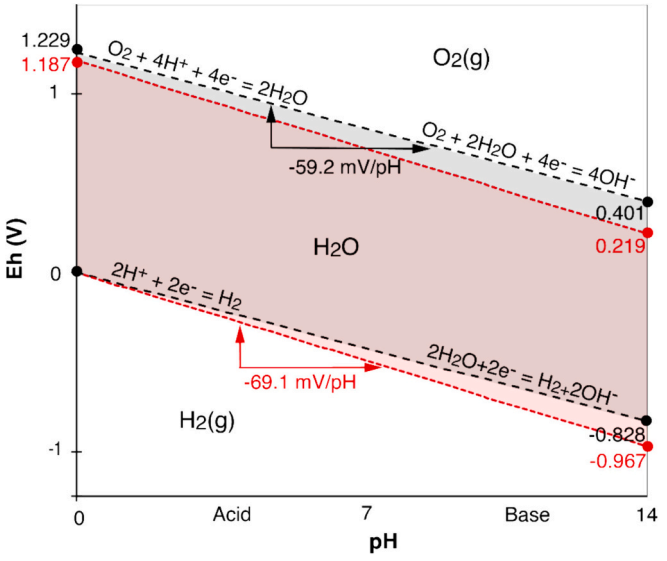

Fig. 1. Pourbaix diagram of water showing its stability field as a function of the redox potential E_h (in V) over the entire pH range, at pO_2 and $pH_2 = 1$. The black and red lines confine the stability field of water at 25 °C and 75 °C, respectively.

one must consider the reduction potential in solution, in particular, whether Eq. (12) can drive HIRCDAMP (or any other reduction for this matter). Thermodynamically, this is indicated by showing a lower electron affinity, i.e., a lower reduction potential, compared to that for carbonate reduction. As Eq. (12) describes the standard hydrogen electrode (SHE), whose reduction potential E^0 is arbitrarily set at 0 V (y-intercept at pH 0 in Fig. 1), any positive reduction potential for a carbonate species is equivalent to the overall cell potential (and thus electromotive force) and indicates a spontaneous reaction. Conversely, a negative reduction potential vs. SHE indicates the opposite, i.e., no thermodynamic driving force for (inorganic) carbon to be reduced to a more organic species. Pertinent standard reduction potentials ($E°$) for the reduction of various carbon species were collated in Table 1.

Standard reduction potentials ($E°$), and consequently derived equilibrium constants K provided in databases, are based on highly *acidic* conditions (pH = 0), in relation to which most HIRCD are thermodynamically favourable. However, reservoirs with carbonates will present rather neutral to alkaline pH conditions, e.g. Bagci et al. (2000); Kharaka and Hanor (2003). Under such basic conditions, it seems more appropriate to use Eq. (14) in Fig. 1. This reaction corresponds conceptually to SHE, but in a one mole OH^- solution (pH 14). Given the alkalising nature of carbonates, this approach of reacting a surplus of hydroxide with dissolved hydrogen appears more appropriate for the ensuing discussion than starting with a pH 0 solution. Note, the reduction potential for Eq. (14) at pH 14 is −0.828 V vs. SHE (y-intercept at pH 14), indicating a strong thermodynamic preference for the oxidation of this half-reaction (i.e., $H_{2(g)}$ to H_2O). It also means the E in Table 1 will shift to more negative values by the same token of 0.828 V (E^-_{OH}) for a pH of 14. As such, the reduction of carbonates under alkaline conditions takes place at more negative reduction potentials. In fact, if Eq. (12) were allowed to proceed as oxidation (i.e., hydrogen loss), and any alkaline carbonate reaction in Table 1 as reduction (as expected by HIRCD), the overall standard cell potential ($E_{cell} = E_r - E_{ox}$) would be equal to E_{OH^-} (=E_r) because E_{ox} of Eq. (12) is 0 V. Based on that hypothetical E_{cell}, the resulting Gibb's free energy of the overall HIRCD at pH 14 (values in bold in Table 1) would be consistently positive and, noticeably, quite large for methane production (last row in Table 1). That would mean an endergonic and non-spontaneous redox reaction for HIRCDAMP, requiring energy to start and sustain. However, the presence and quantity of various gases (and in particular H_2) and other species will also influence the values of the redox potentials in a particular system such as a potential reservoir for UHS. In the following text, the relationship between *Eh* and pH as a function of molal species concentrations has been exploited to map out in more detail the thermodynamic conditions under which HIRCDAMP is favourable. Rather than *Eh*, however, the associated Gibbs free energy change to the system was chosen (Eq. 3).

4. Results and discussion

4.1. Case 1, HIRCDAMP at low H_2 partial pressure

In Fig. 2, the free Gibbs energies of reaction have been computed for five HIRCDAMP cases (see Table 2) using Eqs. (1), (4) with the values of standard free Gibbs energies tabulated in Table 1A (appendix). They represent conditions for a nominal environment composed of a brine at 25 °C and 1 bar, in contact with carbonate minerals (calcite, dolomite, siderite and ankerite). This brine contains Ca^{2+}, Fe^{2+}, $Mg^{2+}$and total inorganic carbon (DIC) at 1 mmol/kg, CH_4(g) at a partial pressure of 1 mbar and H_2(g) at a partial pressure of 1 μbar. Activity coefficients have been taken equal to 1 due to the low ionic strength of the system. Fig. 2 shows that HIRCDAMP is thermodynamically favourable at acidic pH and non-spontaneous at alkaline conditions. To make matters worse, increasing temperatures, such as expected under hydrogen injection, will also decrease reduction potentials. The red dashed lines in Fig. 1 indicate how the stability field of water changes as the slopes dip towards lower *Eh* with increasing pH. This change in slopes stems from the

Table 1
Reduction reactions with corresponding standard reduction potentials related to hydrogen induced (bi)carbonate reduction, Gibbs free energies and logarithmic equilibrium constant *K*. Gibbs free energy at standard conditions of each reduction reaction, ΔG^0, have been computed using Eq. (1) and Gibbs free energies of formation that are listed in Table 1A (appendix). Under alkaline conditions, ΔG is thus positive (in bold font, also reported per reacted mole H_2 in the penultimate column). Standard potentials for the reduction reactions written under acidic conditions (noted E°_{H+}) and under alkaline conditions (noted E°_{OH-}) have then been computed from ΔG^0 and Eq. 10. For E_{OH-}, it is equivalent to subtracting 0.828 V from E°_{H+} (see text for explanation). Overall standard cell potentials (E°_{cell}) have been calculated assuming Eq. (12) as oxidation reaction under acidic conditions ($E^\circ_{ox} = 0$ V) and Eq. (14) under alkaline conditions ($E_{ox} = 0.828$ V), respectively. Under such consistent conditions, E°_{cell} are equal irrespective of the pH. The overall redox reaction (left column) has been added, together with the calculated logarithmic equilibrium constant *K* (Eq. 2) to emphasise the importance of the pH regime for its appropriate expression. The Log *K* in bold font in the last column describes again inconsistent conditions, where E°_{cell} corresponds to E_{OH-}.

Overall redox reaction	Reduction Reaction	E°_{H+} (V)	E^-_{OH} (V)	E_{cell} (V)	ΔG (kJ/mol)	$\Delta G/H_2$ (kJ/mol)	Log *K*
$2HCO_3^- + H_2 = C_2O_4^{-2} + 2H_2O$	$2HCO_3^- + 2H^+ + 2e^- = C_2O_4^{-2} + 2H_2O$	−0.17		−0.170	33	33	−5.7
$2HCO_3^- + H_2 = C_2O_4^{-2} + 2H_2O$	$2HCO_3^- + 2e^- = C_2O_4^{-2} + 2OH^-$		−0.998	−0.170	**193**	193	**−33.7**
$2CO_3^{-2} + H_2 + 2H^+ = C_2O_4^{-2} + 2H_2O$	$2\ CO_3^{-2} + 4H+ + 2e^- = C_2O_4^{-2} + 2H_2O$	0.441		0.441	−85	−85	14.9
$2CO_3^{-2} + H_2 = C_2O_4^{-2} + 2OH^-$	$2\ CO_3^{-2} + 2H_2O + 2e^- = C_2O_4^{-2} + 4OH$-		−0.387	0.441	**75**	75	**−13.1**
$HCO_3^- + H_2 = HCOO^- + H_2O$	$HCO_3^- + 2H^+ + 2e^- = HCOO^- + H_2O$	−0.078		−0.078	15	15	−2.6
$HCO_3^- + H_2 = HCOO^- + H_2O$	$HCO_3^- + H_2O + 2e^- = HCOO^- + 2OH$-		−0.906	−0.078	**175**	175	**−30.6**
$CO_3^{-2} + H_2 + H^+ = HCOO^- + H_2O$	$CO_3^{-2} + 3H^+ + 2e$- $= HCOO^- + H_2O$	0.227		0.227	−44	−44	7.7
$CO_3^{-2} + H_2 = HCOO$- $+ OH^-$	$CO_3^{-2} + 2H_2O + 2e^- = HCOO^- + 3OH^-$		−0.601	0.227	**116**	116	**−20.3**
$HCO_3^- + 2H_2 + H^+ = C + 3H_2O$	$HCO_3^- + 5H^+ + 4e^- = C + 3H_2O$	0.323		0.323	−125	−62	21.8
$HCO_3^- + 2H_2 = C + 2H_2O + OH^-$	$HCO_3^- + 2H_2O + 4e^- = C + 5OH^-$		−0.505	0.323	**195**	97	**−34.1**
$CO_3^{-2} + 2\ H_2 + 2H^+ = C + 3H_2O$	$CO_3^{-2} + 6H^+ + 4e^- = C + 3H_2O$	0.475		0.475	−183	−92	32.1
$CO_3^{-2} + 2H_2 = C + H_2O + 2OH^-$	$CO_3^{-2} + 3H_2O + 4e^- = C + 6OH^-$		−0.353	0.475	**136**	68	**−23.9**
$HCO_3^- + 2H_2 + H^+ = HCOH + 2H_2O$	$HCO_3^- + 5H^+ + 4e^- = HCOH + 2H_2O$	0.044		0.044	−17	−8	3.0
$HCO_3^- + 2H_2 = HCOH + H_2O + OH^-$	$HCO_3^- + 3H_2O + 4e^- = HCOH + 5OH^-$		−0.784	0.044	**303**	151	**−53.0**
$CO_3^{-2} + 2H_2 + 2H^+ = HCOH + 2H_2O$	$CO_3^{-2} + 6H^+ + 4e^- = HCOH + 2H_2O$	0.197		0.197	−76	−38	13.3
$CO_3^{-2} + 2H_2 = HCOH + 2OH^-$	$CO_3^{-2} + 4H_2O + 4e^- = HCOH + 6OH^-$		−0.631	0.197	**244**	122	**−42.7**
$HCO_3^- + 3H_2 + H^+ = CH_3OH + 2H_2O$	$HCO_3^- + 7H^+ + 6e^- = CH_3OH + 2H_2O$	0.107		0.107	−62	−21	10.9
$HCO_3^- + 3H_2 = CH_3OH + H_2O + OH^-$	$HCO_3^- + 5H_2O + 6e^- = CH_3OH + 7OH^-$		−0.721	0.107	**417**	139	**−73.1**
$CO_3^{-2} + 3H_2 + 2H^+ = CH_3OH + 2H_2O$	$CO_3^{-2} + 8H^+ + 6e^- = CH_3OH + 2H_2O$	0.209		0.209	−121	−40	21.2
$CO_3^{-2} + 3H_2 = CH_3OH + 2OH^-$	$CO_3^{-2} + 6H_2O + 6e^- = CH_3OH + 8OH^-$		−0.619	0.209	**358**	119	**−62.8**
$CO_2 + 4H_2 = CH_4 + 2H_2O$	$CO_2 + 8H^+ + 8e^- = CH_4 + 2H_2O$	0.169		0.169	−130	−33	22.9
$CO_2 + 4H_2 = CH_4 + 2H_2O$	$CO_2 + 6H_2O + 8e^- = CH_4 + 8OH^-$		−0.659	0.169	**509**	127	**−89.1**

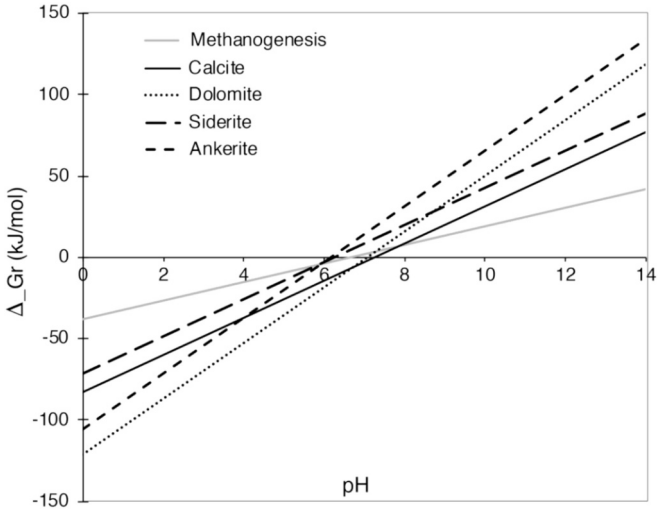

Fig. 2. Change in the Gibbs free energy of reaction as a function of pH for the five HIRCDAMP (hydrogen induced reductive carbonate dissolution and methane production) reactions described in Table 2; $pH_2 = 1$ µbar, $T = 25$ °C.

T-dependence of the thermal voltage given by the Nernst equation and can be calculated as $-2.8e^{-3}$ V/°C for water, under alkaline conditions.

For the carbon system, Ryu et al. (1972) found a temperature gradient of $-1.05e^{-3}$ V/°C for the following pertinent reaction from carbon dioxide to formate:

$$CO_{2(g)} + H_2O + 2\,e^- = HCOO^- + OH^- \quad (15)$$

While this may not seem much, it means a decrease in E^-_{OH} from −0.708 V at 10 °C to −0.760 V at 60 °C and translates into an increase in the already positive ΔG by 10 kJ/mol. Note that a higher partial pressure of CH_4 will increase ΔG similarly. It follows that Eq. (12) is not substantiated by thermodynamic considerations under high pH and *T* regimes, when the partial pressure of H_2 is low.

Table 2
Free Gibbs energies of five carbonate dissolution and methane formation pathways, at standard conditions ($\Delta_r G^o$), and for the nominal environment described in the text. In particular, $pH_2 = 1$ µbar, $T = 25$ °C, pH 7 and 10.

Reactions	Equation	$\Delta_r G^o$ (kJ/mol)	$\Delta_r G_{pH=7}$ (kJ/mol)	$\Delta_r G_{pH=10}$ (kJ/mol)
Methanogenesis	$4H_2(aq) + HCO_3^- + H^+ = CH_4(aq) + 3H_2O$	−230	2	19
Calcite Dissol.	$4H_2(aq) + CaCO_3 + 2H^+ = Ca^{2+} + CH_4(aq) + 3H_2O$	−242	−3	31
Siderite Dissol.	$4H_2(aq) + FeCO_3 + 2H^+ = Fe^{2+} + CH_4(aq) + 3H_2O$	−229	9	43
Ankerite Dissol.	$4H_2(aq) + (Ca,Fe)(CO_3)_2 + 3H^+ = Fe^{2+} + Ca^{2+} + CH_4(aq) + 3H_2O + HCO_3^-$	−229	14	66
Dolomite Dissol.	$4H_2(aq) + (Ca,Mg)(CO_3)_2 + 3H^+ = Mg^{2+} + Ca^{2+} + CH_4(aq) + 3H_2O + HCO_3^-$	−248	−1	50

4.2. Case 2, HIRCDAMP under injection conditions

While increasing pH and *T* create thermodynamic trends unconducive for HIRCDAMP, this observation depends on the amount of hydrogen present and holds only at very low pH_2. With increasing quantities of $H_{2(aq)}$, the ΔG_r-pH system shifts towards more negative, i.e., exergonic conditions under all pH. This is shown in Fig. 3a, an exact copy of Fig. 2 but at 5 bar pH_2. UHS will certainly take place at higher hydrogen pressures where ΔG_r becomes even more negative. This correlation between ΔG_r and pH_2 is based on the fact that, under standard

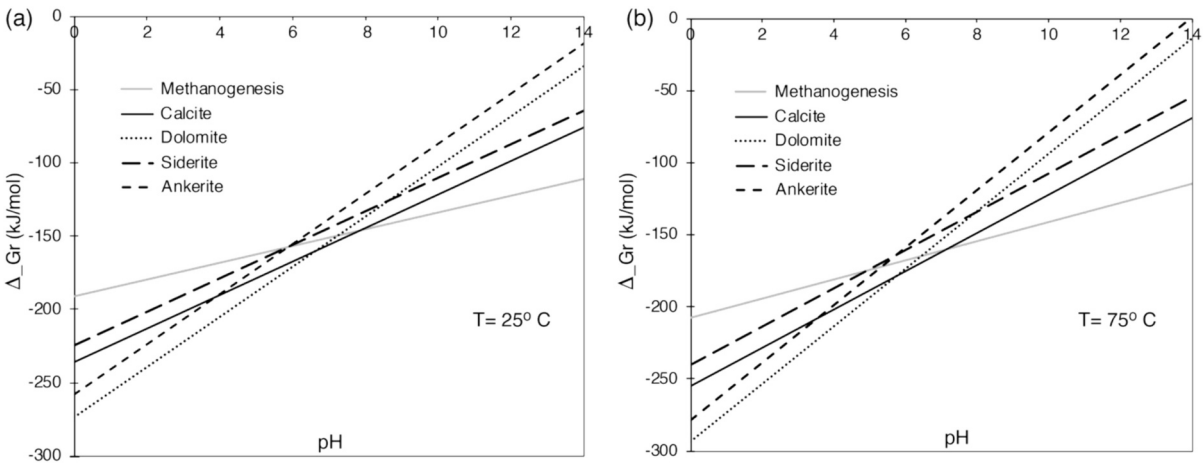

Fig. 3. Change in the Gibbs free energy as a function of pH for the five HIRCDAMP (hydrogen-induced reductive carbonate dissolution and methane production) reactions described in Table 2. (a) $pH_2 = 5$ bar, $T = 25$ °C, (b) $pH_2 = 5$ bar, $T = 75$ °C.

state equilibrium conditions, the equilibrium constant K of Eq. (12) equals the activity of $H_{2(aq)}$ which, in an indefinitely dilute solution and an activity coefficient of one, corresponds to Henry's constant K_H (in mol/kg/bar; $pH_2 = 1$ bar). That is, $K = K_H$.[1] It follows that increasing pH_2 (and $H_{2(aq)}$) will drive Eq. (12) to the left, dissociating and oxidising solvated hydrogen ($H_{2(aq)}$) and creating the protons and electrons required for HIRCDAMP. Raising the temperature to expected reservoir conditions (set arbitrarily at 75 °C in this study) will only marginally raise ΔG_r towards positive values, not enough, however, for HIRCDAMP to become thermodynamically unfavourable again (Fig. 3b) The same result is obtained with a higher CH_4 partial pressure. ΔG will only increase by about 20 kJ/mol when the partial pressure of CH_4 increases from 1 mbar to 5 bars.

It is important to consider here the apparent 'reactivity' of $H_{2(aq)}$ as per Eq. (12). Its low solubility (negative log K_H) means that at equilibrium, more of its atoms are bound as hydronium ions (H_3O^+, left side of Eq. (12)) than as neutral, solvated hydrogen molecules ($H_{2(aq)}$). It is this thermodynamic relationship that creates the driving force behind HIRCDAMP under UHS conditions that is invariably reported in geochemical modelling studies (see the introduction for cited papers). Eq. (12), however, also includes the presence of solvated electrons, destined for the yet oxidised carbonate species. This point is not obvious, though. First off, the lifetime of a solvated electron in water is on the order of (hundreds of) femtoseconds (Migus et al., 1987; Novelli et al., 2023; Wang et al., 2008). This short time window leaves little opportunity to stray too far from the host molecule to find a suitable electron acceptor. Novelli et al. (2023) reported a radius of 2.2 nm for the delocalised solvated electron, which, compared to an effective hydrodynamic radius (Schultz and Solomon, 1961) of a solvated hydrogen molecule of 0.5 nm, (Sabo et al., 2006; Śmiechowski, 2015) allows it only a 2-fold range around the tiny hydrogen molecule ($\sqrt{(2.2/0.5)}$).

Moreover, these and other studies on the solvated electron used radiation energy (radiolysis, photo-ionisation) to remove the electron from the H_2O hydrogen in the first place, i.e., the dissociation of solvated hydrogen is an energy-intensive process. That is, while the reaction in Eq. (12) per se may be thermodynamically favourable, the associated activation energy to extract the electron from its innermost shell is high. One plausible way out of this challenge is the presence of metal and/or organic catalysts which can act as electron acceptors and shuttles (Van der Zee and Cervantes, 2009). It is not hard to imagine how the ephemeral solvated electrons may be captured by the outer membrane of a bacterial cell that is in direct contact with water where it can be shuttled/transferred on to a terminal electron acceptor such as C(+4) (Hernandez and Newman, 2001; Mevers et al., 2019; Pankratova et al., 2019; Ter Heijne et al., 2018; White et al., 2016). After all, experimental and natural examples of hydrogenotrophic methanation (or biomethanation as it is also called) in the presence of inorganic carbon ($CO_{2(aq)}$, HCO_3^-, CO_3^{2-}) below 100 °C abound in the literature (Angelidaki et al., 2011; Dong et al., 2022; Ebigbo et al., 2013; Hagemann et al., 2016; Panfilov, 2010; Shojaee et al., 2024; Strobel et al., 2020; Thapa et al., 2022; Van Eerten-Jansen et al., 2012; Wagner and Ballerstedt, 2013). Note, that the reverse, i.e., methanogenesis inhibition by microorganisms, is also possible (Thaysen et al., 2021; Würdemann et al., 2016).

As a result, even though HIRCDAMP reactions are thermodynamically favourable under UHS conditions during H_2 injection, all published literature has shown that they are kinetically inhibited at such reservoir temperatures unless microorganisms or transition metals acting as catalysts are present, e.g. Jakobsen (2007), Bradley (2016), Lang et al. (2010).

4.3. Case 3, HIRCDAMP along the electron chain

So far, most of the discussion and, to our knowledge, all recent work published on UHS (see the introduction for cited papers) have revolved around HIRCDAMP in the sense of going from the most oxidised form of carbon (+4) to its most reduced form (−4). Fig. 4 shows two carbon Pourbaix plots and illustrates common carbon phases as a function of pH and *Eh*. Both plots were created using the standard reduction potentials calculated from the standard free Gibbs energies compiled in Table 1A and the Nernst equation at 25 °C and molar concentrations of 10^{-3}. To represent the stability field of water, a partial pressure of O_2 of 1 atm was taken for the upper stability limit and three values for the partial pressure of $H_{2(g)}$ (10^{-7} atm, 1 atm and 100 atm) were taken to represent the lower stability limit. Only C(+4), C(0), and C(−4) appear in Fig. 4a as other simple organic carbon species with intermediate oxidation states are deemed metastable with respect to conversion to $CH_{4(g)}$, $CO_{2(g)}$ and H_2O, even in the absence of an oxidant or reductant (Widdel and Musat, 2010). It appears as if HIRCDAMP was a direct, unencumbered path between C(+4) and C(−4), along the electron chain. Yet, this may be an oversimplistic view of what happens in the reservoir. For example, bicarbonate (HCO_3^-) reduction to oxalate ($C_2O_4^{2-}$) involves two electrons (first two rows in Table 1, Fig. 4b) and shows positive Gibbs free energies irrespective of the pH endmember (33 kJ/mol at pH=0 and 193 kJ/mol

[1] The phreeqc database provides a log K of −3.15 for Eqn. (12) whereas the llnl database gives a value of −3.105 for log K_H. The NIST Chemistry Webbook (https://doi.org/10.18434/T4D303) reports log K_H as −3.11, all at 25 °C and 1 bar.

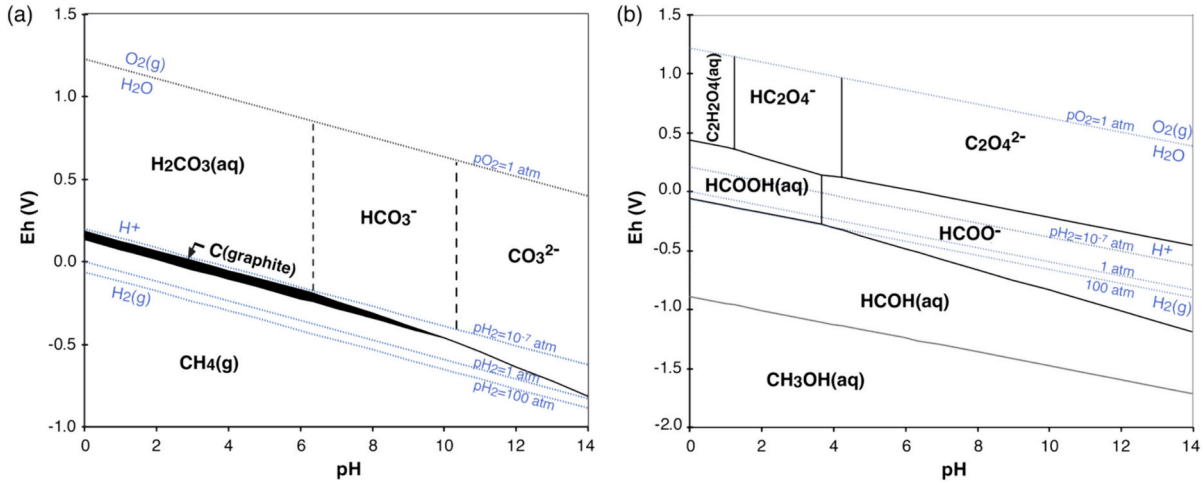

Fig. 4. Carbon Pourbaix plots illustrating carbon phases as a function of pH and *Eh* at 25 °C and molar concentrations of 10^{-3}. (a) Only the most stable carbon phases are represented. Note the small graphite stability field (in black). (b) Metastable carbon phases are depicted.

at pH =14). The same applies to the reduction of bicarbonate to formate ($HCOO^-$), again requiring two electrons (15, 175 kJ/mol). So kick-starting bicarbonate reduction with two electrons is non-spontaneous. If more electrons are involved (e.g., bicarbonate reduction to elemental carbon ($C_{(s)}$) via four electrons) the Gibbs free energy finally becomes negative. This does not signify, however, that the reduction proceeds all the way to methane. The formation of C(0) is kinetically strongly inhibited and has not been observed in abiotic or biotic environments at low temperatures (Widdel and Musat, 2010). Formaldehyde ($HCHO_{(g)}$) may be electrolytically reduced to methanol ($CH_3OH_{(l)}$), but further reduction of methanol does not occur under normal conditions; rather, methanol may be *oxidised* to carbonic acid ($H_2CO_{3(aq)}$) or carbonates (Bard and Ketelaar, 1976). The same source also observes that the $HCOO^-$ group (formic acid, acetic acid) is not reduced at the mercury electrode in aqueous solutions, possibly because electrochemical reactions with carbon are quite slow and need a large overpotential (= electrode potential minus equilibrium potential) to drive them forward. Consequently, at low potential difference between E_r and E_{ox}, the reaction may not even proceed, despite negative Gibbs free energies. Shock (1990) found that kinetic barriers inhibited the approach to stable equilibrium in the C-H-O-N system of submarine hot springs, thus promoting the formation of metastable organic carbon species rather than methane.

This observation was subsequently corroborated in an experimental study of the reaction of $CO_{2(aq)}$ in the presence of olivine under hydrothermal conditions (300 °C, 350 bar). Reduction of $CO_{2(aq)}$ to formate ($HCOO^-_{(aq)}$) via hydrogen oxidation was found to proceed rapidly but further reduction to methane was inconsequential, after more than 2500 h of constant heating (McCollom and Seewald, 2001). A follow-up study (McCollom and Seewald, 2003) showed that reactions between dissolved CO_2 and formate rapidly attained a state of metastable thermodynamic equilibrium, at temperatures of 175 °C to 260 °C, yet again considerably above targeted UHS storage spaces. Another more recent example comes from a hydrothermal field study (McDermott et al., 2015) that found, again, widespread formate formation via $CO_{2(aq)}$ reduction whereas methane production was restricted to H_2-rich fluid inclusions. It follows that at temperatures typical of UHS in depleted reservoirs (e.g., 75 °C), the kinetics of C(+4) reduction to intermediate carbon species are likely to be much slower, indicating that, if at all, the formation of less reduced, metastable species of carbon (especially formate) may govern abiotic hydrogen consumption.

4.4. Case 4, HIRCDAMP in geochemical models

Because Eq. (12) and those compiled in Table 1 are integral parts of the PHREEQC (Parkhurst and Appelo, 2013) thermodynamic databases used almost exclusively in the modelling work published on UHS, it explains why all modelling approaches discussed in the introduction yield invariably methane through carbonate reduction, despite kinetics constraints and unfavourable electrochemical affinity for carbonate reduction to oxalate and formate, respectively vs. SHE at all pHs. To avoid the overall impression of high hydrogen reactivity and consumption in the presence of inorganic carbon, which is inconsistent with experimental observations, PHREEQC allows for the alternative use of unreactive hydrogen as 'Hdg' (among other gases) to express its inertness. That is, instead of using $H_2(g)$ as expression for hydrogen gas, 'Hdg' can used instead which does not participate in any dissociating reactions, unless specifically stipulated. This allows circumventing Eq. (12), yielding modelling results far more aligned with experimental findings. More generally, while geochemical codes initially treated all redox reactions under thermodynamic equilibrium, most codes now allow the decoupling of any (or all) redox species present in the system to take into account redox disequilibrium (Bethke, 2022), which, as demonstrated by Lindberg and Runnells (1984) on more than 600 groundwater samples, is a general behaviour of aqueous systems at low temperatures. Decoupled redox reactions will thus behave independently from the overall redox potential of the system, according to their own reaction kinetics. Recently, an 'uncoupled redox database' was made available to PHREEQC users (https://phreeqcusers.org/index.php?topic=2023.0). These considerations convey the importance of being circumspect when choosing the right frame of modelling. It does not mean that carbonates cannot be reduced, or methane formed, but this will depend on additional factors such as the presence of microbes and/or catalytic surfaces to overcome the activation energy which, using $H_{2(g)}$ in PHREEQC, is taken for granted. If kinetic rates are incorporated into the modelling, they are often only for the dissolutive part of the HIRCDAMP reactions and not the redox part. There are evidently modelling papers that do take microbial reductive activity on UHS into account (Berta et al., 2018; Rotiroti et al., 2018; Shojaee et al., 2024; Veshareh et al., 2022) but those explicitly addressing the reactivity of hydrogen, either by implementing 'Hdg' as a first step (Hemme and van Berk, 2018), discarding abiotic conditions (Tremosa et al., 2023), or suppressing methane formation for being too improbable (Hassannayebi et al., 2019), are still the exception.

Note that the discrepancy between models and experiments is not a matter of time. Admittedly, experiments are run 'only' for weeks or

months at best, rather than tens or hundreds of years applied in simulations to potentially account for the discrepancy in methane sighting. However, extrapolating backward the reported quantities of simulation-based methane to experimental timelines would be plenty to be quantifiable by gas chromatography (GC), capable of analysing traces of this gas. For example, Zeng et al. (2022) simulates 3.1 millimolar annual methane generation from reductive carbonate dissolution which would translate to circa 50 ppmv of methane per month (at 75 °C and 100 bar). This is patently above a regular GC's detection limit for methane.

5. Conclusions

Modelling studies based on purely inorganically mediated HIRCDAMP do not accord with most comparable experimental findings.[2] This paper provides a framework and an explanation of why abiotic hydrogen-driven reductive mobilisation of carbonates and concomitant methane production as per the reactions in Table 2 is unlikely to occur naturally under UHS conditions (in particular, 'low' temperatures, below 60–75 °C). While thermodynamic considerations suggest that ΔG_r, as a measure of the spontaneity of a geochemical reaction, becomes more negative with increasing pH_2, HIRCDAMP is also T and pH-dependent and increasingly less exergonic with increasing T (and thus reservoir depth) and increasing pH (e.g., limestone terrains). By the same token, UHS projects injecting $H_{2(g)}$ with $CO_{2(g)}$ to prompt biomethanation in the underground (Strobel et al., 2020; Wang et al., 2022), have, from a thermodynamic point of view, prospects to prosper. While these studies explicitly count on hydrogenotrophic methanogenesis by archaea, expected to be present in the aqueous phase, the dissolution of $CO_{2(g)}$ in the porewater will create acidic conditions under which abiotic HIRCDAMP is spontaneous under all pH_2 and T conditions anticipated in UHS settings, providing the necessary energy to the microorganisms to drive their metabolism. Thermodynamics also establishes that carbonates may not be comprehensively reduced to methane (even under highly reducing conditions) because reduction is a stepwise process and the first uptake of two electrons is energetically not favourable under any pH regime (and thus reservoir).

Even under conditions where HIRCDAMP is thermodynamically favourable, it may not materialise due to kinetic constraints. The dissociation of hydrogen into protons and electrons (Eq. (12)) requires high (ionisation) energies meaning the associated activation energy is very high and not naturally attained -without catalysts/microbes. Furthermore, this process creates free solvated electrons which have a very short lifespan of femtoseconds and thus spatially a very short range to spread beyond their solvation shell to find a suitable electron acceptor -without microbes acting as electron shuttles. Finally, at low potential difference between both half redox reactions (low overpotential), carbon reduction may not proceed, despite negative Gibbs free energies, because electrochemical reactions with carbon are quite slow and need a large overpotential, i.e., electromotive force, to drive them forward.

Consequently, *abiotic* geochemical modelling studies reporting considerable HIRCDAMP and thus questioning the long-term suitability of carbonate-bearing formations for UHS are likely false positives.

As Zhu and Nordstrom (2022) pointed out in their paper 'Flying Blind: Geochemical Modeling and Thermodynamic Data Files': "Automated software capabilities of computing and graphing cannot be a substitute for the user's basic background and training in thermodynamics, chemical kinetics, interfacial processes, and hydrogeochemistry." The false positives alluded to in this study are a clear example of the importance of this statement. We even go a step further and add that geochemical modelling cannot replace systematic and rigorous experimental work on the hydrogen-brine-rock system to further our understanding, so important for successful medium-term underground storage of hydrogen.

[2] Yes, there are a couple of experimental outliers observing calcite dissolution in the presence of hydrogen (see introduction) but one of that study did not pre-equilibrate their matrix with a hydrogen-free brine prior to their reactivity study (meaning calcite may well have dissolved to re-equilibrate the solution, not due to the presence of hydrogen) and both papers base their findings on anecdotal petrographic observations, not rigorous aqueous geochemistry, let alone gas chromatography to establish unequivocally that HIRCDAMP and hydrogen loss indeed occurred.

CRediT authorship contribution statement

Stephanie Vialle: Writing – review & editing, Visualization, Software, Data curation. **Domenik Wolff-Boenisch:** Writing – original draft, Visualization, Methodology, Conceptualization.

Declaration of competing interest

The authors declare that they have no known competing financial interests or personal relationships that could have appeared to influence the work reported in this paper.

Data availability

Data will be made available on request.

Appendix A. Supplementary data

Supplementary data to this article can be found online at https://doi.org/10.1016/j.chemgeo.2024.122304.

References

Al-Yaseri, A., Al-Mukainah, H., Yekeen, N., 2023. Experimental insights into limestone-hydrogen interactions and the resultant effects on underground hydrogen storage. Fuel 344, 128000.
Angelidaki, I., Karakashev, D., Batstone, D.J., Plugge, C.M., Stams, A.J., 2011. Biomethanation and its potential. In: Methods in Enzymology. Elsevier, pp. 327–351.
Bagci, S., Kok, M.V., Turksoy, U., 2000. Determination of formation damage in limestone reservoirs and its effect on production. J. Pet. Sci. Eng. 28 (1), 1–12.
Bard, A.J., Ketelaar, J., 1976. Encyclopedia of electrochemistry of the elements. J. Electrochem. Soc. 123 (10), 348Ca.
Bensing, J.P., Misch, D., Skerbisch, L., Sachsenhofer, R.F., 2022. Hydrogen-induced calcite dissolution in Amaltheenton Formation claystones: Implications for underground hydrogen storage caprock integrity. Int. J. Hydrog. Energy 47 (71), 30621–30626.
Berta, M., Dethlefsen, F., Ebert, M., Schafer, D., Dahmke, A., 2018. Geochemical effects of millimolar hydrogen concentrations in groundwater: an experimental study in the context of subsurface hydrogen storage. Environ. Sci. Technol. 52 (8), 4937–4949.
Bethke, C.M., 2022. Geochemical and Biogeochemical Reaction Modeling. Cambridge University Press, Cambridge.
Bo, Z., Zeng, L., Chen, Y., Xie, Q., 2021. Geochemical reactions-induced hydrogen loss during underground hydrogen storage in sandstone reservoirs. Int. J. Hydrog. Energy 46 (38), 19998–20009.
Bradley, A.S., 2016. The sluggish speed of making abiotic methane. Proc. Natl. Acad. Sci. USA 113 (49), 13944–13946.
Dong, Z., et al., 2022. Enhanced carbon dioxide biomethanation with hydrogen using anaerobic granular sludge and metal–organic frameworks: Microbial community response and energy metabolism analysis. Bioresour. Technol. 362, 127822.
Ebigbo, A., Golfier, F., Quintard, M., 2013. A coupled, pore-scale model for methanogenic microbial activity in underground hydrogen storage. Adv. Water Resour. 61, 74–85.
Epelle, E.I., et al., 2022. Perspectives and prospects of underground hydrogen storage and natural hydrogen. Sustain. Energ. Fuels 16 (4), 3324–3343.
Flesch, S., Pudlo, D., Albrecht, D., Jacob, A., Enzmann, F., 2018. Hydrogen underground storage—Petrographic and petrophysical variations in reservoir sandstones from laboratory experiments under simulated reservoir conditions. Int. J. Hydrog. Energy 43 (45), 20822–20835.
Gelencsér, O., et al., 2023. Effect of hydrogen on calcite reactivity in sandstone reservoirs: Experimental results compared to geochemical modeling predictions. J. Energy Storage 61, 106737.
Gholami, R., 2023. Hydrogen storage in geological porous media: Solubility, mineral trapping, H2S generation and salt precipitation. J. Energy Storage 59, 106576.
Giardini, A.A., Salotti, C.A., 1969. Kinetics and relations in the calcite-hydrogen reaction and relations in the dolomite-hy-drogen and siderite-hydrogen systems. Am. Mineral.t: J. Earth Planet. Mater. 54 (7–8), 1151–1172.
Hagemann, B., Rasoulzadeh, M., Panfilov, M., Ganzer, L., Reitenbach, V., 2016. Hydrogenization of underground storage of natural gas. Comput. Geosci. 20 (3), 595–606.

Hanley, E.S., Deane, J.P., Gallachóir, B.P.Ó., 2018. The role of hydrogen in low carbon energy futures–a review of existing perspectives. Renew. Sust. Energ. Rev. 82, 3027–3045.
Hassannayebi, N., Azizmohammadi, S., De Lucia, M., Ott, H., 2019. Underground hydrogen storage: application of geochemical modelling in a case study in the Molasse Basin, Upper Austria. Environ. Earth Sci. 78 (5).
Hassanpouryouzband, A., et al., 2022. Geological hydrogen storage: geochemical reactivity of hydrogen with sandstone reservoirs. ACS Energy Lett. 7 (7), 2203–2210.
Heinemann, N., et al., 2021. Enabling large-scale hydrogen storage in porous media – the scientific challenges. Energy Environ. Sci. 14 (2), 853–864.
Hematpur, H., Abdollahi, R., Rostami, S., Haghighi, M., Blunt, M.J., 2023. Review of underground hydrogen storage: Concepts and challenges. Adv. Geo-Energy Res. 7 (2), 111–131.
Hemme, C., van Berk, W., 2018. Hydrogeochemical modeling to identify potential risks of underground hydrogen storage in depleted gas fields. Appl. Sci. 8 (11).
Hernandez, M., Newman, D., 2001. Extracellular electron transfer. Cell. Mol. Life Sci. CMLS 58, 1562–1571.
Jagadeesan, D., Eswaramoorthy, M., Rao, C.N.R., 2009. Investigations of the Conversion of Inorganic Carbonates to methane. ChemSusChem 2 (9), 878–882.
Jakobsen, R., 2007. Redox microniches in groundwater: a model study on the geometric and kinetic conditions required for concomitant Fe oxide reduction, sulfate reduction, and methanogenesis. Water Resour. Res. 43 (12).
Kharaka, Y.K., Hanor, J., 2003. Deep fluids in the continents: I. Sedimentary basins. Treatise Geochem. 5, 605.
Krevor, S., et al., 2023. Subsurface carbon dioxide and hydrogen storage for a sustainable energy future. Nat. Rev. Earth Environ. 4 (2), 102–118.
Lang, S.Q., Butterfield, D.A., Schulte, M., Kelley, D.S., Lilley, M.D., 2010. Elevated concentrations of formate, acetate and dissolved organic carbon found at the lost City hydrothermal field. Geochim. Cosmochim. Acta 74 (3), 941–952.
Lindberg, R.D., Runnells, D.D., 1984. Ground water redox reactions: an analysis of equilibrium state applied to Eh measurements and geochemical modeling. Science 225 (4665), 925–927.
Mao, G.-C., et al., 2022. Alkaline earth metal-induced hydrogenation of the CaO-captured CO2 to methane at room temperature. Ind. Eng. Chem. Res. 61 (28), 10124–10132.
McCollom, T.M., Seewald, J.S., 2001. A reassessment of the potential for reduction of dissolved CO2 to hydrocarbons during serpentinization of olivine. Geochim. Cosmochim. Acta 65 (21), 3769–3778.
McCollom, T.M., Seewald, J.S., 2003. Experimental constraints on the hydrothermal reactivity of organic acids and acid anions: I. Formic acid and formate. Geochim. Cosmochim. Acta 67 (19), 3625–3644.
McDermott, J.M., Seewald, J.S., German, C.R., Sylva, S.P., 2015. Pathways for abiotic organic synthesis at submarine hydrothermal fields. Proc. Natl. Acad. Sci. USA 112 (25), 7668–7672.
Mevers, E., et al., 2019. An elusive electron shuttle from a facultative anaerobe. eLife 8, e48054.
Migus, A., Gauduel, Y., Martin, J.L., Antonetti, A., 1987. Excess electrons in liquid water: first evidence of a prehydrated state with femtosecond lifetime. Phys. Rev. Lett. 58 (15), 1559–1562.
Miocic, J., et al., 2023. Underground hydrogen storage: a review. Geol. Soc. Lond. Spec. Publ. 528 (1), SP528-2022-88.
Muhammed, N.S., et al., 2022. A review on underground hydrogen storage: Insight into geological sites, influencing factors and future outlook. Energy Rep. 8, 461–499.
NIST, 2013. National Institute of Standards and Technology: Reference Fluid Thermodynamic and Transport Properties Database (REFPROP): Version 8.0. https://www.nist.gov/srd/refprop.
Novelli, F., et al., 2023. The birth and evolution of solvated electrons in the water. Proc. Natl. Acad. Sci. USA 120 (8), e2216480120.
Pan, B., Yin, X., Ju, Y., Iglauer, S., 2021. Underground hydrogen storage: Influencing parameters and future outlook. Adv. Colloid Interf. Sci. 294, 102473.
Panfilov, M., 2010. Underground Storage of Hydrogen: In Situ Self-Organisation and Methane Generation. Transp. Porous Media 85 (3), 841–865.
Pankratova, G., Hederstedt, L., Gorton, L., 2019. Extracellular electron transfer features of Gram-positive bacteria. Anal. Chim. Acta 1076, 32–47.
Parkhurst, D.L., Appelo, C., 2013. Description of input and examples for PHREEQC version 3—a computer program for speciation, batch-reaction, one-dimensional transport, and inverse geochemical calculations. US Geol. Survey Techniques Methods 6 (A43), 497.
Peng, W., et al., 2021. Abiotic methane generation through reduction of serpentinite-hosted dolomite: Implications for carbon mobility in subduction zones. Geochim. Cosmochim. Acta 311, 119–140.
Raza, A., et al., 2022. A holistic overview of underground hydrogen storage: Influencing factors, current understanding, and outlook. Fuel 330, 125636.
Reitenbach, V., Ganzer, L., Albrecht, D., Hagemann, B., 2015. Influence of added hydrogen on underground gas storage: a review of key issues. Environ. Earth Sci. 73 (11), 6927–6937.
Rönsch, S., et al., 2016. Review on methanation – from fundamentals to current projects. Fuel 166, 276–296.
Rotiroti, M., Jakobsen, R., Fumagalli, L., Bonomi, T., 2018. Considering a threshold energy in reactive transport modeling of microbially mediated redox reactions in an arsenic-affected aquifer. Water 10 (1).
Ryu, J., Andersen, T., Eyring, H., 1972. Electrode reduction kinetics of carbon dioxide in aqueous solution. J. Phys. Chem. 76 (22), 3278–3286.
Sabo, D., Rempe, S.B., Greathouse, J.A., Martin, M.G., 2006. Molecular studies of the structural properties of hydrogen gas in bulk water. Mol. Simul. 32 (3–4), 269–278.
Sambo, C., et al., 2022. A review on worldwide underground hydrogen storage operating and potential fields. Int. J. Hydrog. Energy 47 (54), 22840–22880.
Schultz, S.G., Solomon, A.K., 1961. Determination of the effective hydrodynamic radii of small molecules by viscometry. J. Gen. Physiol. 44 (6), 1189–1199.
Scott, H.P., et al., 2004. Generation of methane in the Earth's mantle: in situ high pressure-temperature measurements of carbonate reduction. Proc. Natl. Acad. Sci. 101 (39), 14023–14026.
Shock, E.L., 1990. Geochemical constraints on the origin of organic compounds in hydrothermal systems. Orig. Life Evol. Biosph. 20 (3), 331–367.
Shojaee, A., Ghanbari, S., Wang, G., Mackay, E., 2024. Interplay between microbial activity and geochemical reactions during underground hydrogen storage in a seawater-rich formation. Int. J. Hydrog. Energy 50, 1529–1541.
Śmiechowski, M., 2015. Molecular hydrogen solvated in water – a computational study. J. Chem. Phys. 143 (24).
Strobel, G., Hagemann, B., Huppertz, T.M., Ganzer, L., 2020. Underground bio-methanation: Concept and potential. Renew. Sust. Energ. Rev. 123, 109747.
Tarkowski, R., 2019. Underground hydrogen storage: Characteristics and prospects. Renew. Sust. Energ. Rev. 105, 86–94.
Tarkowski, R., Uliasz-Misiak, B., 2022. Towards underground hydrogen storage: a review of barriers. Renew. Sust. Energ. Rev. 162, 112451.
Ter Heijne, A., de Rink, R., Liu, D., Klok, J.B., Buisman, C.J., 2018. Bacteria as an electron shuttle for sulfide oxidation. Environ. Sci. Technol. Lett. 5 (8), 495–499.
Thapa, A., Park, J.-G., Jun, H.-B., 2022. Enhanced ex-situ biomethanation of hydrogen and carbon dioxide in a trickling filter bed reactor. Biochem. Eng. J. 179, 108311.
Thaysen, E.M., et al., 2021. Estimating microbial growth and hydrogen consumption in hydrogen storage in porous media. Renew. Sust. Energ. Rev. 151.
Thiyagarajan, S.R., Emadi, H., Hussain, A., Patange, P., Watson, M., 2022. A comprehensive review of the mechanisms and efficiency of underground hydrogen storage. J. Energy Storage 51, 104490.
Tremosa, J., Jakobsen, R., Le Gallo, Y., 2023. Assessing and modeling hydrogen reactivity in underground hydrogen storage: a review and models simulating the Lobodice town gas storage. Front. Energy Res. 11, 1145978.
Van der Zee, F.P., Cervantes, F.J., 2009. Impact and application of electron shuttles on the redox (bio)transformation of contaminants: a review. Biotechnol. Adv. 27 (3), 256–277.
Van Eerten-Jansen, M.C.A.A., Heijne, A.T., Buisman, C.J.N., Hamelers, H.V.M., 2012. Microbial electrolysis cells for production of methane from CO2: long-term performance and perspectives. Int. J. Energy Res. 36 (6), 809–819.
Veshareh, M.J., Thaysen, E.M., Nick, H.M., 2022. Feasibility of hydrogen storage in depleted hydrocarbon chalk reservoirs: Assessment of biochemical and chemical effects. Appl. Energy 323, 119575.
Wagner, M., Ballerstedt, H., 2013. Influence of bio-methane and hydrogen on the microbiology of underground gas storage. Literature study; Einfluss von Biogas und Wasserstoff auf die Mikrobiologie in Untertagegasspeichern. Literaturstudie. Technical Report DGMK-756, ISBN 978-3-941721-36-4.
Wang, C.R., Luo, T., Lu, Q.B., 2008. On the lifetimes and physical nature of incompletely relaxed electrons in liquid water. Phys. Chem. Chem. Phys. 10 (30), 4463–4470.
Wang, G., Pickup, G., Sorbie, K., Mackay, E., 2022. Numerical analysis of bio-methanation process during underground hydrogen storage. EAGE GET 2022 2022 (1), 1–5.
White, G.F., et al., 2016. Chapter three - mechanisms of bacterial extracellular electron exchange. In: Poole, R.K. (Ed.), Advances in Microbial Physiology. Academic Press, pp. 87–138.
Widdel, F., Musat, F., 2010. Energetic and other quantitative aspects of microbial hydrocarbon utilization. In: Handbook of Hydrocarbon and Lipid Microbiology, pp. 729–763.
Würdemann, H., Halm, H., Lerm, S., Kleyböcker, A., 2016. Verbund-Forschungsvorhaben H2STORE: Untersuchung der geohydraulischen, mineralogischen, geochemischen und biogenen Wechselwirkungen bei der Untertage-Speicherung von H2 in konvertierten Gaslagerstätten: Teilprojekt 4-Mikrobiologie: Abschlussbericht: Berichtszeitraum: 01.08. 2012 bis 31.12. 2015. Helmholtz-Zentrum Potsdam Deutsches GeoForschungsZentrum GFZ.
Yoshida, N., Hattori, T., Komai, E., Wada, T., 1999. Methane formation by metal-catalyzed hydrogenation of solid calcium carbonate. Catal. Lett. 58 (2), 119–122.
Zeng, L., Keshavarz, A., Xie, Q., Iglauer, S., 2022. Hydrogen storage in Majiagou carbonate reservoir in China: Geochemical modelling on carbonate dissolution and hydrogen loss. Int. J. Hydrog. Energy 47 (59), 24861–24870.
Zeng, L., et al., 2023. Storage integrity during underground hydrogen storage in depleted gas reservoirs. Earth Sci. Rev., 104625
Zhan, S., Zeng, L., Al-Yaseri, A., Sarmadivaleh, M., Xie, Q., 2024. Geochemical modelling on the role of redox reactions during hydrogen underground storage in porous media. Int. J. Hydrog. Energy 50, 19–35.
Zhu, C., Nordstrom, D.K., 2022. Flying blind: geochemical modeling and thermodynamic data files. Groundwater 60 (6), 699–700.
Zivar, D., Kumar, S., Foroozesh, J., 2021. Underground hydrogen storage: a comprehensive review. Int. J. Hydrog. Energy 46 (45), 23436–23462.